MEASUREMENT OF THE THIRD-ORDER NONLINEAR REFRACTIVE INDEX OF VANADIUM OXIDE NANOSCROLLS

By

Charles H. Adams

Thesis

Submitted to the faculty of the

Graduate School of Vanderbilt University

in partial fulfillment of the requirements

for the degree of

MASTER OF SCIENCE

in

Physics

December 2012

Nashville, Tennessee

Approved:

Richard F. Haglund, Jr.

James H. Dickerson II

Norman H. Tolk

ABSTRACT

Vanadium dioxide is a strongly correlated electronic material which undergoes a phase transition from a semiconducting to metallic state when illuminated with an intense electric field. This phase transition marks interest in using VO_2 as an optical limiter In this work, the z-scan method is used to find the third order nonlinear index n_2 of VO_x nanoscrolls prepared via a sol-gel method and then suspended in a liquid. The nonlinear index is then compared to the third order nonlinear index of multi-wall carbon nanotubes (also suspended in a liquid), and gold nanoparticles implanted in glass. Both the VO_x nanoscrolls and multi-wall carbon nanotubes have similar n_2, while the gold nanoparticles exhibit a much larger nonlinear index.

ACKNOWLEDGEMENTS

Research was supported by the DOE, ITT AES, DOD US Army, NSF/STTR/Kent Optronics, Northrop Grumman, and NSF. A special thank you to Dr. Benjamin W. Schmidt, who produced the VO_x nanoscrolls as well as the XPS stoichiometry data. I would also like to thank my advisor, Richard Haglund, my committee, and my mother, Kathy Adams.

TABLE OF CONTENTS

Page

TABLE OF CONTENTS

Page

LIST OF FIGURES Page

Chapter I

INTRODUCTION

MOTIVATION

Many vanadium oxides are optically active, spurring interest in using these materials in such ways as solar heat control, opto-electronic devices, photonic computing, and optical limiting[1-4]. In order to understand how best to use these materials, it is useful to understand how they react to high intensities of photons, when nonlinear effects such as intensity-dependent absoption and refraction become important. These comprise two of the third-order nonlinear optical effects observable under intense illuminations[5]. Materials of particular interest are those that undergo a phase transition, such as many of the vanadium oxides[1].

Vanadium pentoxide is a low mobility n-type super conductor, with polycrystalline films exhibiting multicolored electrochromism and photochromism, and is a candidate material for thin film batteries and chemical detectors[6]. Even more usefully, the material can be reduced to other oxide states of vanadium, such as VO_2 or V_2O_3, both of which undergo a metal-insulator transition, VO_2 at 340 K and V_2O_3 at 150 K[6-8].

Of particular interest is vanadium dioxide, a strongly correlated electronic material that undergoes a phase transition from a semiconducting monoclinic state to a metallic tetragonal state when the temperature of the material is raised above 340K[8, 9]. This phase transition can also be induced optically by an intense light source such as a laser beam. This has sparked interest in using VO_2 as an optical limiter, a third order effect also known as intensity-dependent transmission. There are many methods of VO_2 thin film deposition such as sputtering, pulsed laser deposition, and e-beam deposition[8, 9]. Another solution to

incorporating the properties of VO_2 into films on the surface involves nanoparticles of VO_2 be suspended in a polymer solution, which is then applied to a surface and allowed to dry[10]. Upon drying, the resulting film would have the optical limiting properties of VO_2 with an easy application process. Furthermore, the optical properties of nanoscale VO_2 of various geometries have been explored in the literature, from nanodisks[11, 12] to nanobeams[13] to (in the case of this work) nanoscrolls.

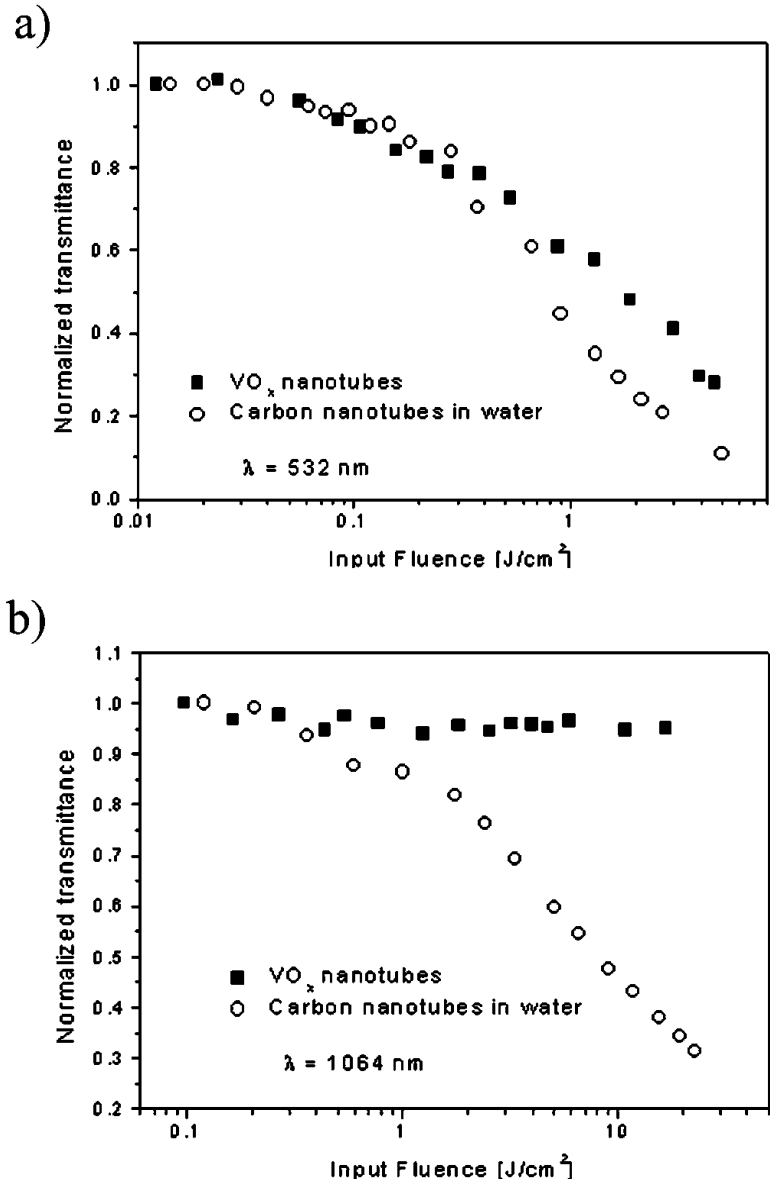

Figure 1 – Xu, et al., Transmittance vs. fluence of VO_x nanotubes and multi-wall carbon nanotubes at a) 532 nm and b) 1064 nm[10].

These scrolls are not stoichiometric VO_2, however; the chemical synthesis process followed by Krumeich, et al.[14], and by Dr. Benjamin Schmidt here at Vanderbilt University produces stoichiometries closer to V_2O_5. The nonlinear optical properties of the material are still of interest, however, since ntensity-dependent transmission measurements by Xu, et al., have already published on using VO_x nanoscrolls as an optical limiter. In their work, they measured the intensity dependent transmission of nanoscrolls suspended in water using a ns Nd:YAG laser at 532 nm and 1064 nm. Figure 1 shows the results of their experiment. The vanadium oxide nanotubes show similar intensity dependent transmission to multi-wall carbon nanotubes at 532 nm; however at 1064 there is almost no optical limiting observed with the nanoscrolls. The authors posit that this is because the bandgap of their nanoscrolls is 2.7 eV, the 1064 nm (1.16 eV) light is not energetic enough to excite two-photon absorption, which is the cause of the strong intensity dependent transmission of the VO_x nanoscrolls when illuminated by 532 nm light. It is this two-photon absorption, along with the nonlinear refraction are the effects that govern how light is transmitted through the suspension of nanoscrolls[10].

NONLINEAR OPTICS

In this work, the nonlinear index of refraction and the nonlinear absorption of several materials are measured using a ns Nd:YAG laser. The nonlinear index can be understood by considering that when an electric field is applied to a material, a dipole moment is induced[5]. This polarization depends on both the fundamental properties of the material and the applied electric field and can be expressed as a Taylor expansion in terms of the electric field E:

$$P = \varepsilon_0(\chi^{(1)}E + \chi^{(2)}E^2 + \chi^{(3)}E^3 + \ldots) \quad (1)$$

where P is the polarization, ε_0 is the permittivity of free space, χ is the susceptibility of the material, and E is the electric field. With small electric fields, only the term containing $\chi^{(1)}$ need be considered, but once the electric field becomes sufficiently large, such as a focused laser beam like that used in this experiment, the effects of the higher order susceptibility terms come into play. Because the experiments are run on nanotubes and nanoscrolls in solution, inversion symmetry dictates that for isotropic media, $\chi^{(2)}$ must be zero. So the third order susceptibility becomes the first nonzero nonlinear term. Similiarly to $\chi^{(2)}$, for an isotropic medium, $\chi^{(4)}$ must be zero, and while the electric field of the Nd:YAG laser is strong, it is not strong enough that the fifth order susceptibility can be significant. Therefore the polarization of the medium can be given by:

$$P = \varepsilon_0 E\left[\chi^{(1)} + \chi^{(3)} E^2\right] \tag{2}$$

An effective susceptibility, χ_{eff}, can be defined such that:

$$\chi_{eff} = \chi^{(1)} + \chi^{(3)} E^2 \tag{3}$$

which can be related to the index of refraction, n, by the following:

$$n^2 = 1 + \chi_{eff} \tag{4}$$

The intensity-dependent index of refraction can be written as a combination of the linear index and an intensity-dependent part.

$$n = n_0 + n_2 I \tag{5}$$

where I is the intensity, n_0 is the linear index of refraction, and n_2 is the nonlinear index of refraction. Furthermore, equation (5) may be substituted into equation (4). Given that $n_2 I << n_0$ for this experiment, $(n_2 I)^2$ need not be included in the expansion of n^2. That leaves

$$n_0^2 + 2 n_0 n_2 I = 1 + \chi^{(1)} + \chi^{(3)} E^2 \tag{6}$$

The constant terms n_0^2 and $1+\chi^{(1)}$ are necessarily equal to one another. Also, the electric field and the intensity are related by $I = 2n_0\varepsilon_0 cE^2$. It is then possible to express the nonlinear index in terms of the susceptibility of the material.

$$n_2 = \frac{\chi^{(3)}}{4n_0^2\varepsilon_0 c} \tag{7}$$

where c is the speed of light. This means that the nonlinear index of refraction is directly proportional to the third-order susceptibility of the material in an electric field[5].

The second nonlinear process that is possible in the material is two-photon absorption. With a large enough intensity, the probability that a photon further excites an electron that has already been excited into a short-lived virtual state becomes significant. This absorption occurs in addition to the linear absorption, so the intensity dependent absorption coefficient can be expressed as:

$$\alpha = \alpha_0 + \beta I \tag{8}$$

Where α is the absorption coefficient, α_0 is the linear absorption coefficient and β is the nonlinear absorption coefficient[5].

MECHANISMS OF NONLINEAR INDEX

The nonlinear index can be observed via several mechanisms including electronic polarization, thermal effects, and electrostriction. Electronic nonlinearities arise due to the distortion of the electron cloud by the applied electric field. In dielectric materials, this effect is typically very fast and small compared to other mechanisms since it involves only virtual processes. However, for a system involving metallic nanoparticles implanted in a dielectric, such as gold implanted in silica, the excitation of plasmons in the metal by the laser are much

larger oscillations of the electrons. They are also involve real processes. This could then lead to a larger electronic polarization contribution to the refractive index of the material[5].

In contrast to electronic polarization mechanisms, thermally induced changes in the nonlinear index can be rather large. Thermal effects are observed in the nonlinear index when some of the laser energy is absorbed into the material, thereby raising the temperature of the illuminated portion. Because the temperature of the material is greater, the electrons have a larger thermal energy and this change in temperature manifests as a change in the index of refraction of the material. This can arise from long-term CW illumination, which could steadily heat the material, or insufficient time for the sample to cool between laser pulses[5].

Electrostriction causes dielectric materials to become compressed when experiencing a strong electric field. Molecules experiencing the electric field are drawn to the region of increasing field strength. This results in a change in the density of the material that then affects the dielectric constants. When, as in this work, the electric field is applied by a laser inside a liquid dielectric medium, the molecules of the liquid are compressed into the region of the laser beam. The higher the power at a particular region, the more the molecules will be compressed, and the more the index of refraction will change. Therefore the maximum change of index of refraction will occur near the along the z-axis of the laser beam[5, 15]. Furthermore, mesoscopic objects within the liquid medium, such as dielectric microspheres, can be trapped toward the central axis of the laser beam, further altering the index of refraction[16]. This phenomenon can be exploited to create optical tweezers[17].

Chapter II

Z-SCAN EXPERIMENT AND METHODOLOGY

Z-SCAN THEORY

A Z-scan experiment measures the nonlinear index and absorption. Unlike other methods for measuring the nonlinear index of a material, such as four-wave mixing, Z-scan gives both the magnitude and the direction of the nonlinear index, n_2 [18].

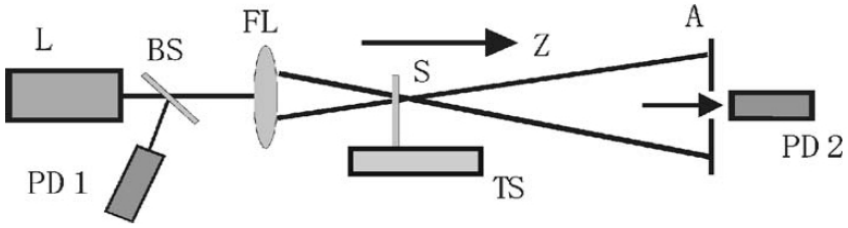

Figure 2 – Z-scan experiment[18]

A Z-scan experiment is set up as in figure 2. A portion of the beam is diverted to a detector before the sample to account for fluctuations in laser intensity. The transmission through the sample is measured by a second detector, and the intensity measured by detector 2 can be divided by the intensity measured by detector 1 to obtain a normalized transmission curve. The laser beam is focused by a lens and the sample is moved through the focal plane, where the intensity of laser light experienced by the sample is a function of the distance (z) from the focal plane of the sample. An aperture in front of detector 2 can be opened and closed to control how much of the beam being measured. The open-aperture configuration refers to the case when the aperture does not obscure any of the light that has passed through the sample so that all of the light is measured by the detector. The closed-aperture configuration refers to the case when the aperture obscures the light passing through the sample that deviates significantly from the z-axis of the experiment.

In order to distinguish between effects due to nonlinear refraction and those due to nonlinear absorption, both open aperture and closed aperture measurements must be made. In the case of the open aperture, the contribution of the nonlinear absorption to the transmission measurement is observed. In the case of the closed aperture scan, both the contribution of the nonlinear refraction and the nonlinear absorption can be observed. The measured transmission is affected by the nonlinear refraction because, as the sample moves through the focal plane, the changing index of refraction changes the radius of the beam transmitted through the sample. This manifests as a change in the beam radius at the closed aperture, where only light propagating along the z-axis is transmitted through the closed iris. This can be measured by a small change in the phase of the laser pulse transmitted through the sample. The equation for a Gaussian laser pulse is:

$$E(z,r,t) = E_0(t)\frac{w_0}{w(z)}\exp\left(-\frac{r^2}{w^2(z)} - \frac{ikr^2}{z(1+z_0^2/z^2)}\right)e^{-i\varphi(z,t)} \tag{9}$$

where E is the electric field, E_0 is the electric field at the focus of the beam, w_0 is the radius of the beam at the focus, w(z) is the beam radius as a function of z, k is the wave number, $z_0 = kw_0^2/2$ is the Rayleigh length of the beam, φ contains the radially uniform phase variation. As a function of z, we get for changes in φ:

$$\Delta\varphi(z,t) = \frac{\Delta\Phi_0(t)}{1+z^2/z_0^2} \tag{10}$$

where $\Delta\Phi_0$ is the on-axis phase shift at the focus. $\Delta\Phi_0$ is defined as:

$$\Delta\Phi_0(t) = k\Delta n_0(t)L_{eff} \tag{11}$$

where k is again the wave number, $\Delta n_0(t) = n_2 I(t)$ contains the nonlinear index n_2, and $L_{eff} = \left(1-e^{-\alpha L}\right)/\alpha$ is the effective length, in which L stands for the length of the sample, and

α is the linear absorption coefficient. However, the experiment measures the intensity of transmitted light, not the electric field. By calculating the quotient of the intensity measured by detector 1 divided by detector two, one obtains the relative transmission T(z):

$$T(z) = \frac{\int_{-\infty}^{\infty} P_T(\Delta\Phi_0(t))dt}{S\int_{-\infty}^{\infty} P_i(t)dt} \tag{12}$$

where P_T is the transmitted power measured on detector 2 and P_i is the input power measured on detector 1. S is the linear aperture transmittance, and is given by:

$$S = 1 - \exp\left(-\frac{2r_a^2}{w_a^2}\right) \tag{13}$$

where r_a is the radius of the aperture and w_a is the radius of the beam at the aperture. w_a therefore depends on how the radius of the beam is changed by the nonlinear index of refraction. If the distance to the detector is sufficiently larger than the Rayleigh length z_0, and the aperture size is small enough such that $S \approx 0$, then the term $\Delta\Phi_0$ can be found by fitting the normalized transmission with the following equation:

$$T(z,\Delta\Phi_0) = 1 - \frac{4\Delta\Phi_0 x}{(x^2+9)(x^2+1)} \tag{14}$$

where $x = z/z_0$[18]. The previous equation is valid for thin samples, where the length of the sample, $L << z_0$. In the case where the sample thickness is on the order of z_0, different fitting conventions need to be adapted, because the sample can be modeled as a series of thin lenses. This introduces an aberration coefficient $a = 6.4(1-S)^{0.35}$. This formula was found experimentally by Sheik-Bahae, et al. For $S \approx 0$, as is the case in this experiment, this correction factor reduces to a = 6.4, and is included in the fitting function[19]:

$$T(z,\Delta\Phi_0) = 1 + \frac{4\Delta\Phi_0 x}{a(x^2+1)^2} \tag{15}$$

For the nonlinear absorption, the open aperture scan can be fitted with the following equation:

$$T_{OA}(z,q_0) = \frac{\ln\left(1+q_0/(1+x^2)\right)}{q_0/(1+x^2)} \tag{16}$$

where $q_0 = \beta I_0 L_{eff}$ contains the nonlinear absorption coefficient β and I_0, L_{eff}, and $x = z/z_0$ as defined above[20].

DESCRIPTION OF SAMPLES MEASURED

The nonlinear index of three different samples was measured: VO_x nanoscrolls in solution, multi-wall carbon nanotubes (MWCNTs) in solution, and gold nanoparticles implanted in SiO_2.

The VO_x nanoscrolls consist of multiple layers of vanadium spaced by an amine layer. In order to create A solution of vanadium(V) triisopropoxide and a primary amine (C_nH_{2n}+1NH_2 with $4 \le n \le 22$) or a R,ö-diamine (H_2N-$[CH_2]_n$-NH_2 with $14 \le n \le 20$) in a molar ratio of 2:1 in anhydrous ethanol (3 mL/g of vanadium precursor) was stirred under inert atmosphere for 1 h. The resulting yellow solution of the alkoxide-amine adduct was hydrolyzed with water (5 mL/g of vanadium precursor) under vigorous stirring. After aging (12-96 h), an orange composite of surfactant and hydrolyzed vanadium oxide component was obtained. The hydrothermal reaction of this composite in an autoclave at 180 °C for 7 days resulted in a black product. It was finally washed with ethanol and hexane to remove residues of unreacted amine or decomposition products and then dried at 80 °C (1 d) under vacuum[14]. X-ray photo-electron spectroscopy measurements by Dr. Schmidt suggest these scrolls are closer to V_2O_5 than to the other oxidation states of vanadium.

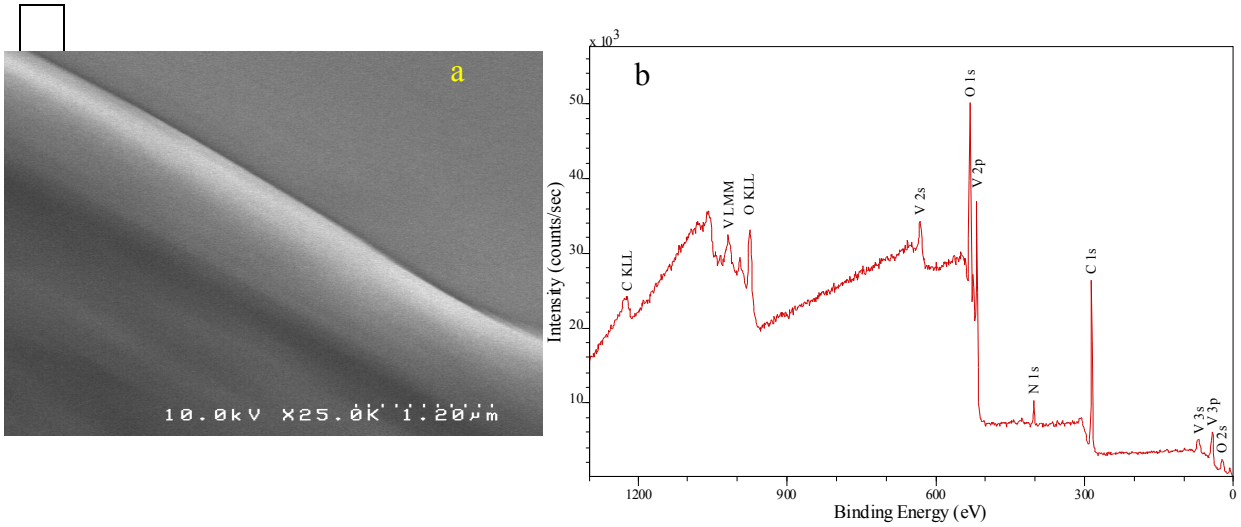

Figure 3 -- (a) SEM image of a VO_x nanoscroll. (b) XPS spectrum of VO_x nanoscrolls measured by Dr. Schmidt.

X-ray photoelectron spectroscopy works by irradiating a material with x-rays, then measuring the energies of core electrons that have been ionized from the atoms in the material. The stoichiometry of a sample can be determined by measuring the counts in the peaks of an XPS spectrum such as the one shown in figure 3(b). Literature suggests that these scrolls can be reduced to VO_2 and V_2O_3[21].

The MWCNTs were commercially obtained from SES Reasearch and have a length distribution of 5-15 µm and a radius distribution of 40-60 nm. The purity is >95% with a remainder of 1-2 µm nanotubes, ash and amorphous carbon[22].

Nanotubes and nanoscroll colloidal suspensions were obtained by adding 25 mg nanotubes or nanoscrolls to a 5% solution of sodium dodecylsulfate solution in deionized water and then sonicated for six hours. The solution was then pipetted to a glass cuvette for the optical measurement.

The SiO_2-implanted gold consists of an implanted layer is approximately 100 nm thick and the gold particles are of the order 10 nm in size, with 10% metal.

Z-SCAN EXPERIMENT

In order to measure the nonlinear index n_2 of the VO_x nanoscrolls, an automated z-scan experiment was constructed which resembles the experiment described in Sheik-Bahae[18]. Figure 4 shows a block diagram of the z-scan apparatus. For easy alignment purposes, the experiment is mounted on an optical rail. At each end of the rail is an iris to facilitate alignment. Iris 2 also serves the function of the aperture in figure 2, being fully open in the open aperture configuration as described above, and closed to all but the on axis light in the closed aperture configuration. The light from the laser passes through Iris 1, through a Glen-Laser polarizer mounted on a Thorlabs mechanical rotation stage model PRM1Z8. The 532 nm light exits the laser polarized vertically, so rotating the polarizer between 0^o and 90^o degrees controls the initial intensity of the laser beam passing through the experiment. The light then passes through a nonpolarizing 50:50 beam splitter, where half is collected by silicon detector B, and recorded by the Picoscope™. The remaining light is focused by a 50 mm focal length lens onto the sample mounted on a 50 mm Thorlabs translation stage model MTS50-Z8. Finally the light transmitted through the sample passes through Iris 2 and is collected by silicon detector A and is also recorded by the Picoscope™.

The light source is a Continuum Minilite™ Nd:YAG laser operating in the second harmonic at 532 nm. The Nd:YAG laser operates by flashlamp pumping; when the flashlamp is pulsed electronically, it excites Nd atoms in the Nd:YAG gain medium to an excited state. In the absence of a Q-switch, photons can reenter the rod causing stimulated emission, leading to a wide high energy pulse. A Q-switch consisting of a crystal quarter wave plate and a horizontal polarizer is used to improve peak power and energy by not allowing photons to reenter the cavity. When the Q-switch is closed, it blocks stimulated

emission which allows the number of excited atoms in the rod to build. When opened, the cavity's stored energy is released very quickly, resulting in high peak power. While the q-switch closed, horizontally polarized light exiting the rod cannot return to stimulate emission because the polarization of light passing through the quarter waveplate and subsequently reflected back into the tube is rotated 90^0, so it is blocked by the horizontal polarizer. Furthermore, vertically polarized light is automatically blocked by the horizontal polarizer. After about 200 μs the is Q-switch opened by a high voltage placed across the wave plate, which then rotates the light an additional 90^0 which means that horizontally polarized light returned as horizontally polarized light and is free to oscillate between the cavity end mirrors, and release the energy stored within, giving 5 ns pulse duration. Internal triggering for both the flashlamp and the Q-switch was selected and the flashlamp was allowed to fire at 15 Hz, the highest repetition rate available for the laser, in the interests of stability[23].

The emitted light from the Nd:YAG laser is at the 1064 nm wavelength. For the experiment 532 nm wavelength light for the experiment was obtained by second-harmonic generation by passing the light through a frequency doubling crystal. Second harmonic generation is a second order nonlinear optical process, and is possible because the crystal is not an isotropic medium, and the second order susceptibility ($\chi^{(2)}$) is nonzero[5]. Second-harmonic generation occurs when two 1064 nm photons collinearly enter the crystal with the same circular polarization. The two photons excite an electron to a virtual state, which quickly decays to a single electron with twice the frequency and the sum of the angular momentum of the two 1064 nm photons. In this case, the emitted 532 nm photon has vertical polarization and having been created by a second-order nonlinearity, is used to probe a third-order nonlinearity[23].

The data from the two detectors are collected in a Pichotech Picoscope™ 3206B. The translation stage, rotation stage, and Picoscope are controlled by a LabVIEW™ program written for that purpose (Appendix A). The LabVIEW™ program is capable of collecting an arbitrary number of transmission measurements for an arbitrary number (limited by the resolution of the stage, memory of the picoscope, and memory of the computer) of translation stage or rotation stage positions. For measurments made until the present, only sweeps of the translation stage have been done, leaving the rotation stage in a fixed position. For every sample, measurements were made with iris 2 in the closed aperture and open aperture configurations. The data are then recorded into text files to be analyzed in MATLAB™.

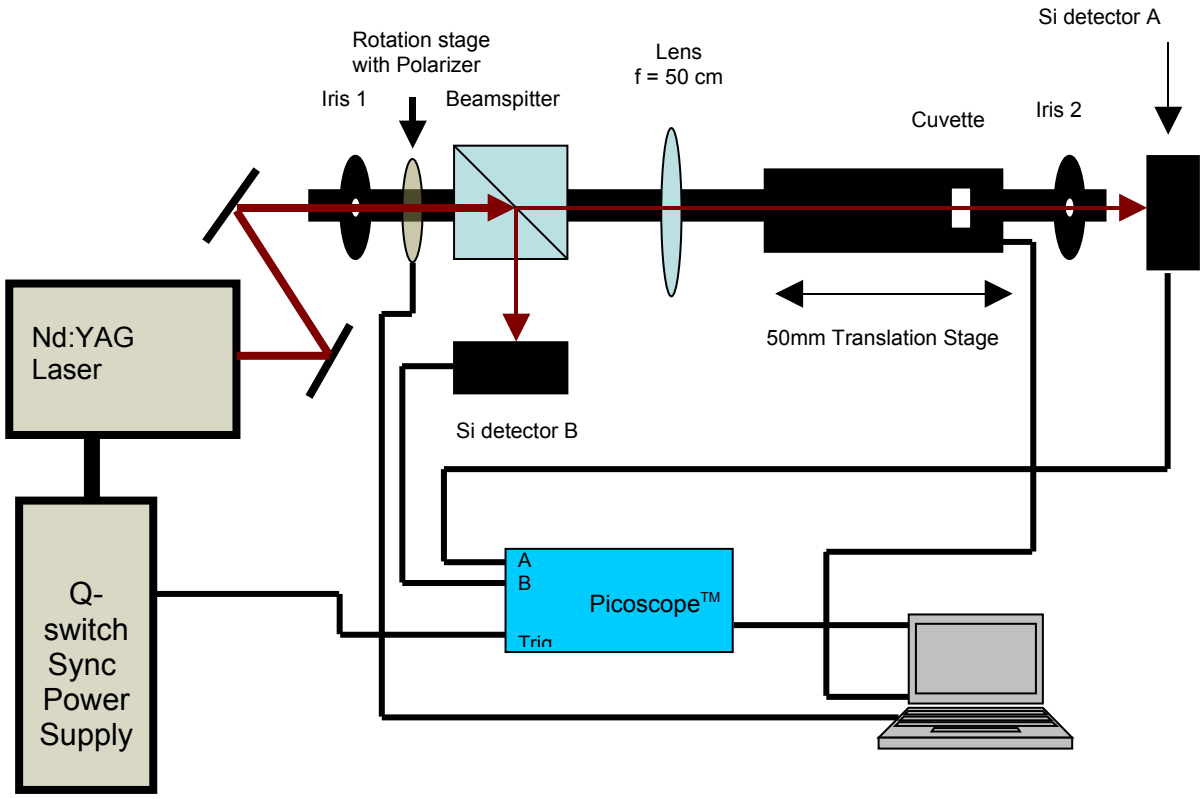

Figure 4 – Block diagram of z-scan experiment used in this work

ANALYSIS OF Z-SCAN IN MATLAB™

The Picoscope data collected by the LabVIEW™ program were exported in a folder of text files, one text file for every picoscope measurement. The program also output a list of translation stage positions at which the transmission was measured. This could lead to two to four thousand text files to be analyzed for each experiment. Therefore, a MATLAB™ script (Appendix B) was developed to automate the analysis of the text files. This script averaged the intensity data from both detectors for each stage position, and calculated the normalized transmission by dividing the average intensity from detector A by the average intensity from detector B for each stage position. The script then plotted the normalized transmission versus position for the scan. This was done in both the open aperture and closed aperture configurations. The scan could then be fitted using a nonlinear least squares fit in MATLAB™'s curve fitting tool to determine β and n_2[24].

To determine the nonlinear absorption, the open aperture scan was fit with the equation:

$$T_{OA} = a\left[\frac{\ln\left(1+\frac{q_0}{1+(z-d)^2/z_0^2}\right)}{\frac{q_0}{1+(z-d)^2/z_0^2}}\right] \tag{17}$$

Resembling equation (16), where T_{OA} is the open aperture transmission (i.e. intensity from detector A divided by intensity from detector B), a is a normalizing factor, q_0 is the term containing the nonlinear absorption coefficient, z is the position of the translation stage, z_0 is the Rayleigh length, and d is the position of the focal plain relative to the position of the translation stage. Since $q_0 = \beta I_0 L_{eff}$, the fit then yields a value for β for a known intensity and effective length. For the VO_x nanoscrolls and MWCNTs in suspension, the difference in

intensity transmitted through an empty cuvette and a full cuvette distant from the focus of the lens was very small, it can be assumed that αL is small. Given $L_{eff} = \left(1 - e^{-\alpha L}\right)/\alpha$, the expansion of $e^{-\alpha L}$ can be written as Taylor expansion to the first order as $e^{-\alpha L} \approx 1 - \alpha L + \ldots$. For small αL this means then that $L_{eff} \approx [1 - (1 - \alpha L)]/\alpha$ or $L_{eff} \approx L$. This is not the case, however, for the film of gold nanoparticles implanted in silica. These exhibit strong linear absorption, and so L_{eff} must be calculated.

To calculate the nonlinear index, the contribution of the nonlinear absorption to closed aperture transmission measurements must be eliminated. That can be achieved by dividing the normalized transmission from the closed aperture scan by the normalized transmission from the open aperture scan. For the optically thick samples (i.e. the suspensions of nanoscrolls and nanotubes), the resulting data can then be fitted with the equation:

$$T_{CA/OA} = A\left(1 + \frac{4\Delta\Phi_0((z-d)/z_0)}{a((z-d)^2/z_0^2 + 1)^2}\right) \tag{18}$$

Resembling equation (15) where $T_{CA/OA}$ is the closed aperture transmission divided by the open aperture transmission, $\Delta\Phi_0 = k\Delta n_0 L_{eff}$, A is a normalizing factor, a is the aberration coefficient, z is the stage position, z_0 is the Rayleigh length, and d is the focal plane position relative to stage position. The fit actually gives a value for $\Delta\Phi_0/a$, so the aberration factor (6.4 in the case of these experiments) must be taken into consideration, so the fit gives $\Delta\Phi_0 = a(k)\Delta n_0 L_{eff}$. This is not the case for the gold nanoparticles, since the sample is optically thin, so equation (14) is used to fit the transmission data.

KNIFE-EDGE MEASUREMENTS

Because both q_0, $\Delta\Phi_0$, and Δn_0 all depend on the intensity at the focal plane, measurements of I_0 are needed. The knife-edge measurement measures the intensity of the laser beam as it is gradually eclipsed by a sharp surface (hence knife-edge) perpendicular to the beam axis. As the eclipsing surface travels into the beam path, the intensity measured at detector A is decreased as more and more of the beam is blocked. This was accomplished by turning the translation stage such that it moved perpendicular to the beam axis, mounting a razorblade on the stage, and modifying the LabVIEW™ z-scan program to make knife-edge measurements at several points over a range of a few millimeters along the beam path between the lens and detector A. The LabVIEW™ modifications were necessary because, while the z-scan program was designed to take measurements along the entire 50 mm range of the translation stage, it only took 1-3 mm of stage movement to be sure the laser beam went from fully unblocked to fully blocked by the razorblade.

For a Gaussian beam:

$$w(z)^2 = w_0^2\left(1+\left(\frac{(z-d)}{z_0}\right)^2\right) \tag{19}$$

where w(z) is the beam radius, w_0 is the beam radius at the focal spot, z is the distance from the lens, d is the distance of the focal plane from the lens, and $z_0 = \pi w_0^2/\lambda$ is the Rayleigh length.

Since the intensity measured by detector A is the integral of the beam intensity as a function of position (in this case, x), it can be described by:

$$I(x) = A\int_x^{\infty} e^{-(x-x_0)^2/w(z)^2}\,dx \tag{20}$$

where I is the intensity measured, A is a constant, x is the stage position, x_0 is the center of the beam relative to stage position, and w(z) is the 1/e beam radius at distance z from the lens. By taking the numerical derivative of I(x):

$$\frac{dI(x_i)}{dx_i} = \frac{I(x_{i+1}) - I(x_i)}{x_{i+1} - x_i} \tag{21}$$

and fitting the resultant Gaussian using MATLAB™'s curve fitting tool, I was able to obtain the value of w(z). The measurement was then repeated for several values of z before and after the focal plane. Figure 5 shows the beam radius measurements squared versus z position. To obtain w_0, the values for w(z) can be fitted with the parabola $w(z)^2 = az^2 + bz + c$. From this, and equation (19), equivalences for a, b, and c in terms of w_0, z_0, and d are derived. Completing the square for $w(z)^2$ gives:

$$w(z)^2 = \left(c - \frac{b^2}{4a}\right) + a\left(x + \frac{b}{2a}\right)^2 = w_0^2\left(1 + \left(\frac{(z-d)}{z_0}\right)^2\right) \tag{22}$$

From here it becomes clear that $w_0^2 = c\text{-}b^2/(4a)$, $z_0^2 = 1/a$, and $d = -b/(2a)$. From this fit, for a 50 cm lens, a beam radius $w_0 = 15$ μm is obtained. For an laser pulse of several mJ, this will give an intensity on the order of 10^9 W/cm^2.

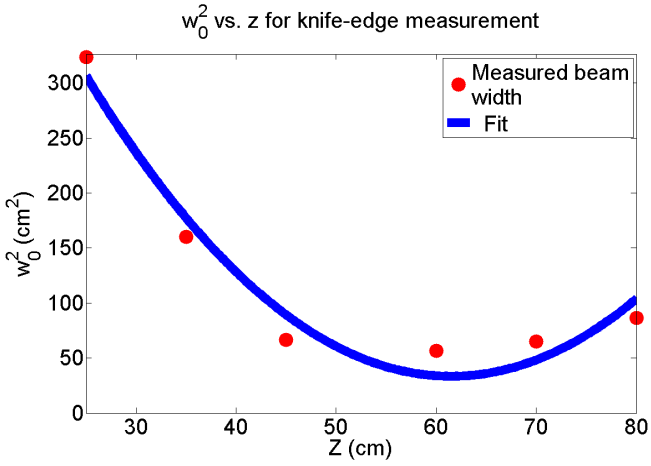

Figure 5 – Beam radius vs. z for 50 cm lens

The poor fit can be attributed to the fact that the beam seems to deviate somewhat from a Gaussian shape throughout the knife-edge measurement process. Appendix C shows the knife-edge measurements at multiple distances from the focal lens.

Chapter III

Z-SCAN RESULTS.

MULTI-WALL CARBON NANOTUBES

Both the open-aperture and closed-aperture transmission through multi-wall carbon nanotubes in solution were taken at 0.5 mm steps as the stage traversed its entire range. At each position, 40 transmission measurements were collected and averaged to obtain the transmission for that position. The laser intensity was calculated to be 5.3×10^9 W/cm^2 at the focus from a power measurement of the unfocused laser beam using the beam radius of 15 μm obtained from the knife-edge measurements. The focal spot was measured to be at z = 25 mm. Figure 6 shows the plot of measured open aperture transmission versus position for multi-wall carbon nanotubes and the fit of the data to equation (17). A value for $q_0 = 0.068$ was obtained. From the relation $q_0 = \beta I_0 L_{eff}$, using $L_{eff} \approx L = 5$cm, a value of $\beta = 2.6 \times 10^{-9}$ cm/W was obtained.

Figure 6 shows the closed aperture measurements for the multi-wall carbon nanotubes. It has the same shape as the open aperture transmission measurements, indicating that the nonlinear absorption still is the dominant factor in the intensity-dependent transmission. In order to deconvolute the two processes, the transmission from the closed aperture measurement will be normalized by that of the open aperture measurement shown in figure 7, along with the fit to equation (18).

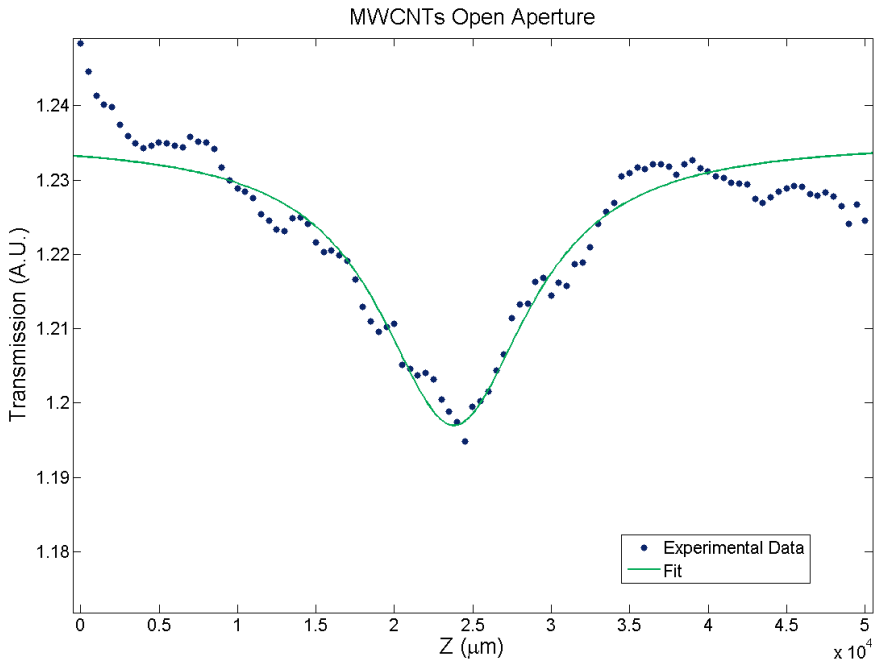

Figure 6 – Open-aperture z-scan of multi-wall carbon nanotubes and fit to equation (17)

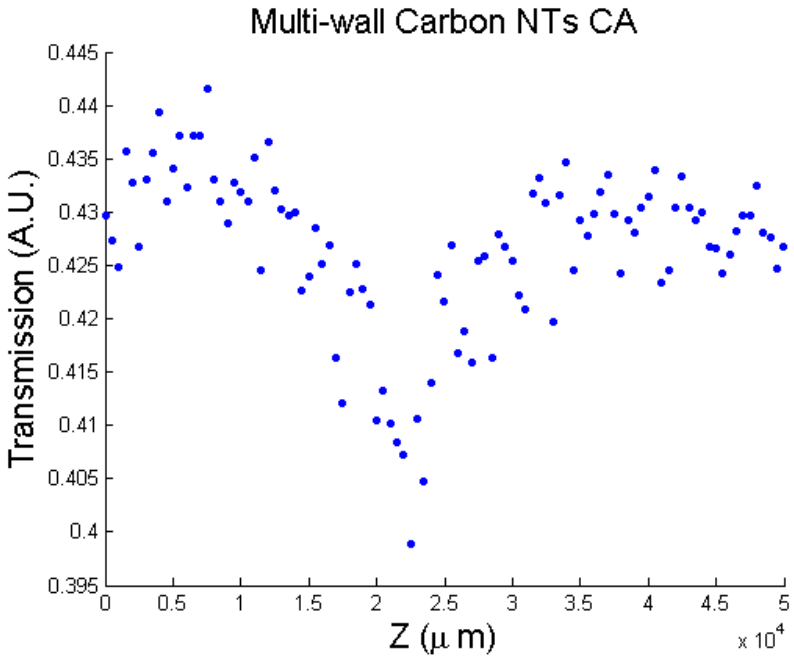

Figure 7—Closed-aperture z-scan of multi-wall carbon nanotubes

Of several measurements, figures 6-8 represent the best effort to date measuring the transmission through MWCNTs in suspension. Figure 8 shows valley typically associated with an intensity dependent index of refraction. However, past the focus the peak is missing. Giving further concern is the broad feature centered at z = 10 mm. It could be noise, given that the actual change in nonlinear index and nonlinear absorption (which govern the shape of these curves) is small. That explanation is unsatisfactory in that it seems to be some kind of trend rather than evenly distributed about y = 0.35 as would be expected from noise. Given that a scan lasts 40 minutes, it could be some result of the nanotubes settling in the solution. A ready explanation for either the lack of peak or the feature at 10 mm does not present itself. Future scans will be devoted to eliminating both of these problems.

However, being the best measurement to date of T_{CA}/T_{OA} for multi-wall carbon nanotubes it was fit it to equation (18) to get a value of $\Delta\Phi_0/a = 0.023$. For $\Delta\Phi_0 = (\Delta n_0)kL_{eff}$ and taking the value of a = 6.4, as well as $k = 2\pi/532nm$ and the same L_{eff} as for the open aperture scan, I obtained a value for $\Delta n_0 = 2.5x10^{-6} = n_2 I_0$. For I_0 the same as the open aperture value, this gives $n_2 = 4.7x10^{-16}$ cm^2/W.

As mentioned in the Mechanisms section, when illuminated by the laser, the molecules of the liquid medium and the nanotubes are compressed in the area illuminated by the laser[15]. Because the nanotubes are rather large, the change in index due to the electrostrictive force should be small, compared to say, the embedded gold nanoparticles, as a significant electric field would be required to appreciably overcome the inertia of the nanotubes. The time-domain of a nanosecond laser pulse also corresponds well with the electrostrictive force[5]. Furthermore, it is possible that the nanotubes work to align

themselves with the electric field of the laser. The contribution of this effect could be determined by comparisons between the n_2 of the nanotubes and fullerene.

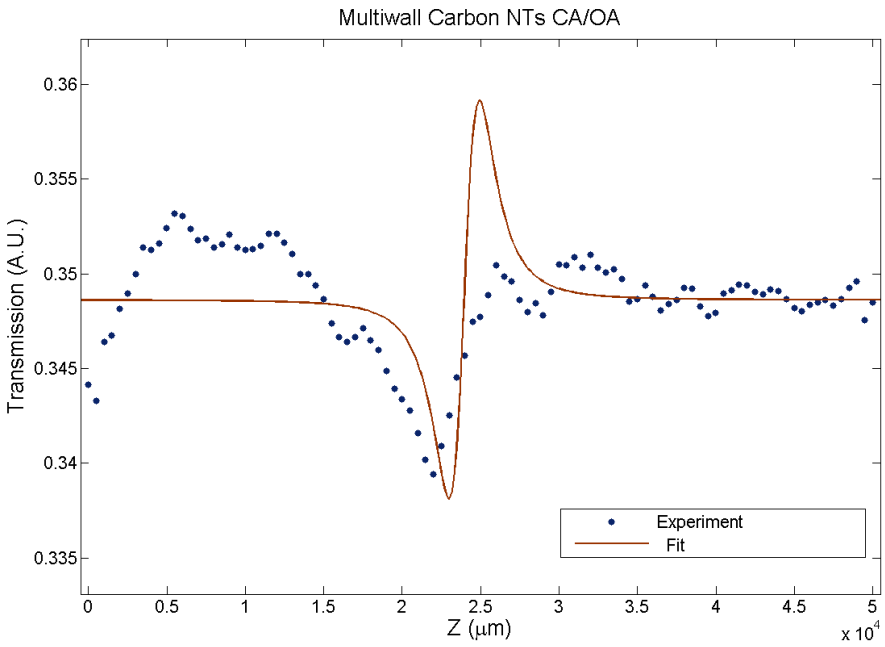

Figure 8 – T_{CA}/T_{OA} for multi-wall carbon nanotubes as well as fit to equation (18)

VO_X NANOSCROLLS

Both the open-aperture and closed-aperture transmission through VO_x nanoscrolls in solution were taken at 1 mm steps as the stage traversed its entire range. At each position, 40 transmission measurements were collected and averaged to obtain the transmission for that position. The laser intensity was calculated to be 7.2×10^9 W/cm^2 at the focus from a power measurement of the unfocused laser beam using the beam radius of 15 μm obtained from the knife-edge measurements. The focal spot was measured to be at z = 25 mm. Figures 9 and 10 show the closed- and open-aperture scans for VO_x nanoscrolls. Both scans have the same basic shape, with a large peak centered at about z = 30 mm. Were there some kind of saturation effects, one would expect them to be centered at the focus, where the intensity is

strongest. As with the MWCNTs, a ready explanation for this is lacking. However, if the closed aperture transmission is normalized by the open aperture transmission, the familiar peak and valley appear. Fitting to equation (18) gives a $\Delta\Phi_0/a = 0.022$. $\Delta\Phi_0 = (\Delta n_0)kL_{eff}$, $k = 2\pi/532nm$, $L_{eff} \approx 5$ cm, and $a = 6.4$ this gives $\Delta n_0 = 2.4x10^{-6}$. Substituting in the intensity at the focus in $\Delta n_0 = n_2 I_0$ gives an nonlinear index $n_2 = 3x10^{-16}$ cm^2/W.

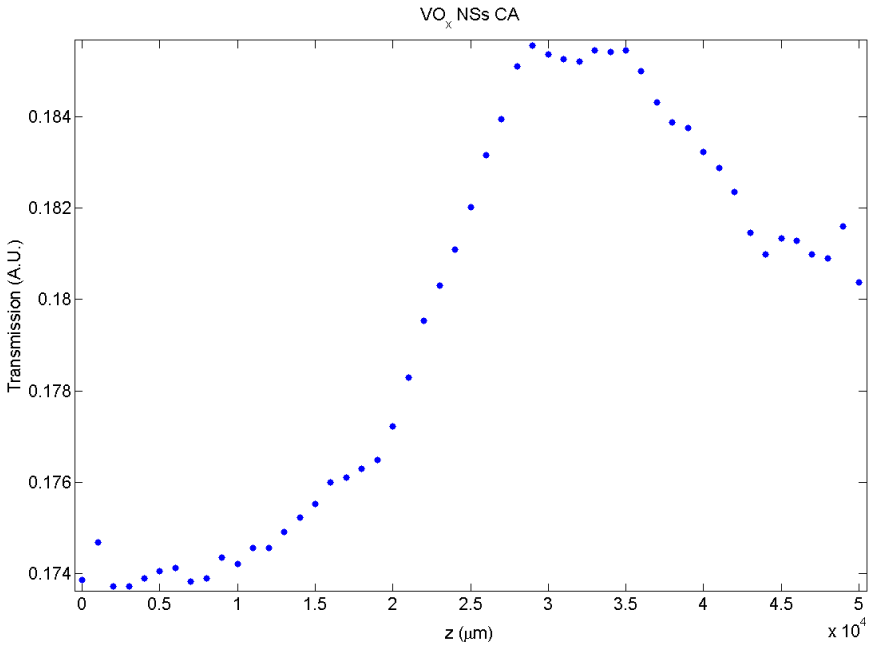

Figure 9 – Closed aperture transmission of VO_x Nanoscrolls

The nonlinear index of both the carbon nanotubes and the VO_x nanoscrolls are similar in order of magnitude. This implies that the same mechanism is responsible for the change in refractive index for both materials. Given the time-scale of nanoseconds and that the nanotubes and –scrolls are suspended in solution, it is likely that the electrostrictive force contributes to n_2. However, it is unknown the effects laser-induced heating may have on the nanoscroll or -tube solutions. It is possible that the contributions to n_2 from heating dwarf those due to electrostriction. Further experimentation and simulations will be needed to determine the mechanisms responsible for the Δn. Furthermore, it is unclear whether an

induced dipole the VO_x nanoscrolls will work to align them with the laser field. A comparison to spherical V_2O_5 nanoparticles in suspension would help determine if a dipole-dipole interaction exists.

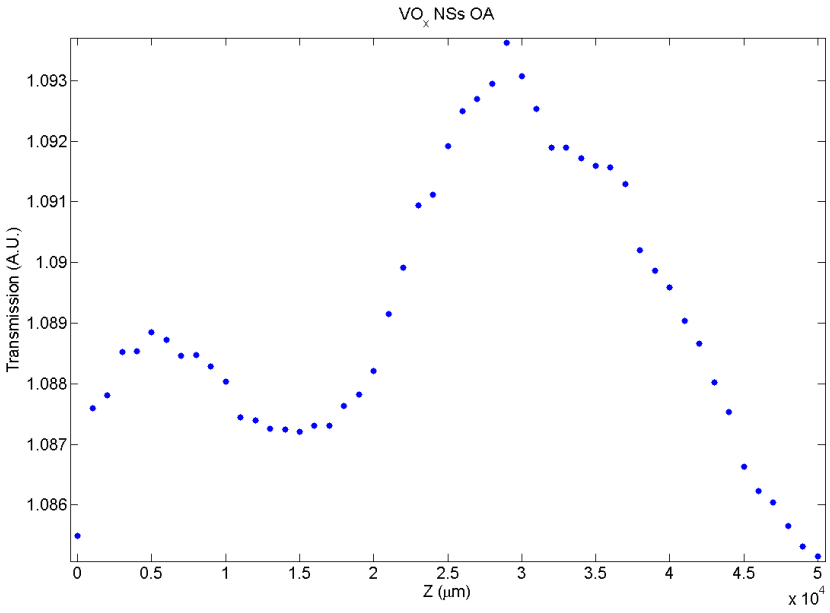

Figure 10 – Open aperture transmission of VO_x Nanoscrolls

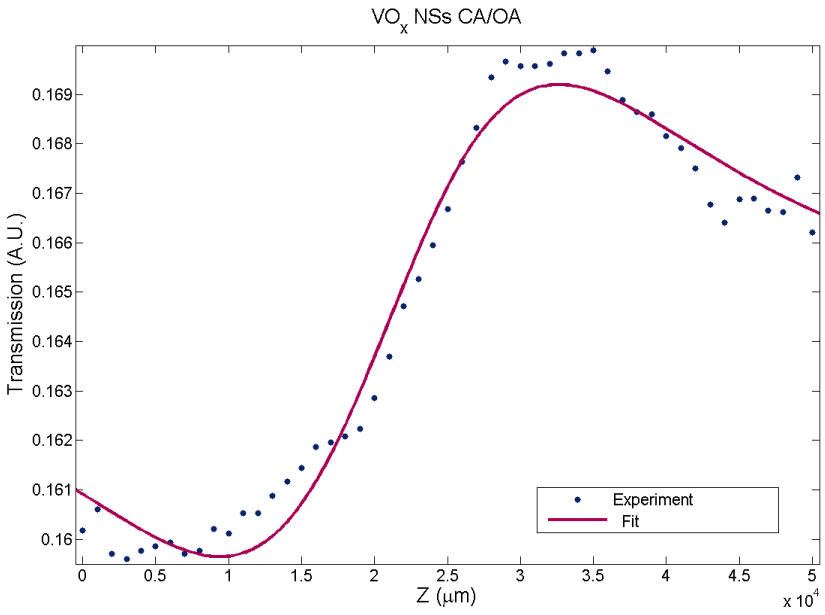

Figure 11 – T_{CA}/T_{OA} for VO_x nanoscrolls as well as fit to equation (18)

This small change in index due to electrostriction can be compared to a plasmonic system. At a time when I was having trouble measuring the nonlinear index of the MWCNTs and VO_x nanoscrolls, Prof. Haglund provided a sample of gold nanoparticles implanted in silica in order to test the experiment on a sample that had been known to show intensity dependent refraction. Initially in trying to measure the nonlinear index of the gold, the laser was operated at the same power as with the nanotubes and –scrolls. However, it was quickly discovered that intensity damaged the sample, so the maximum needed to be reduced by two orders of magnitude. Given a focal spot size of 15 μm, the intensity was measured at 7.5×10^7 W/cm^2.

As with the VO_x nanotubes, both the closed and open aperture scans show a strong peak in the transmission at a position away from the focal plane, in this case at z = 15 mm. And as with the VO_x nanotubes, a ready explanation for the peak and for its location is lacking. However, once again, the T_{CA}/T_{OA} (figure 14) normalization reveals the valley and peak indicative of a change in the index of refraction. Fitting to equation (14), I obtained a value of $\Delta\Phi_0 = 0.21$. In the equation $\Delta\Phi_0 = (\Delta n_0)kL_{eff}$, $k = 2\pi/532$ nm, but more importantly, α is not small in this case, so the $L_{eff} \neq L$, from measurements in the unfocused beam, I obtained $\alpha L = 1.1$. From the definition $L_{eff} = (1-e^{-\alpha L})/\alpha$, it was a simple matter to calculate L_{eff} = 61 nm. From that I obtained $\Delta n_0 = 0.29$. Using the measured intensity, this means that the nonlinear index $n_2 = 4 \times 10^{-9}$ cm^2/W. This agrees well with an almost identical experiment performed by Ryasnyanskiy, et al., which yielded for gold nanoparticles implanted in SiO_2 $n_2 = 3 \times 10^{-9}$ cm^2/W. Their measurements were performed on gold implanted in silicon with a mean particle size of 2.6 nm and 8% metal[25, 26] with a Nd:YAG laser with a 532 nm

wavelength and a 7ns pulse duration[26]. Furthermore, the authors go on to demonstrate that the n_2 they observed was due purely to an electronic effect, caused when the laser excited plasmons in the gold nanoparticles[26]. Though effects due to laser-induced heating cannot be ruled out, the similarities of the two experiments were such that the changes in n_2 can be contributed in part to electronic effects.

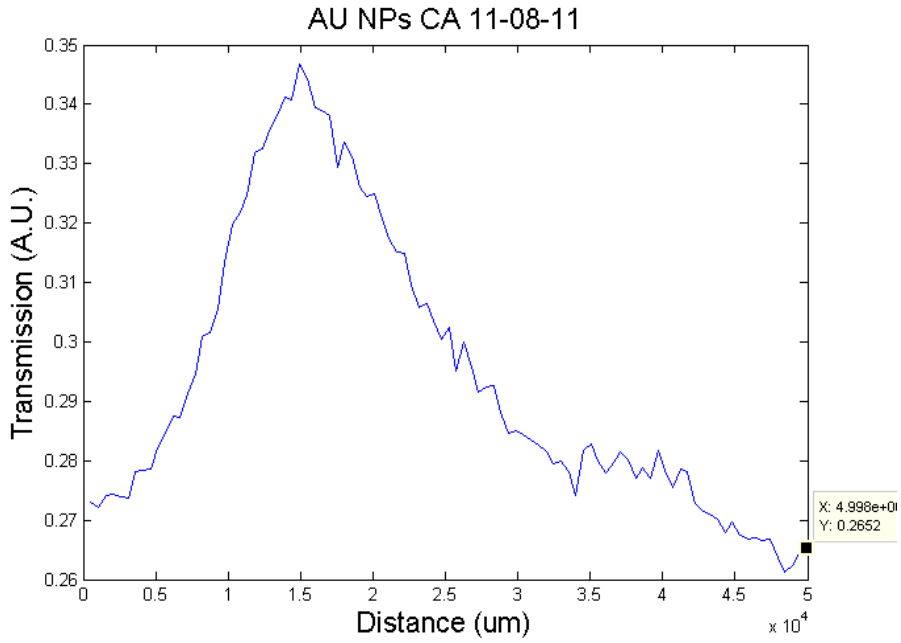

Figure 12 – Closed aperture scan of gold nanoparticles imbedded in SiO_2

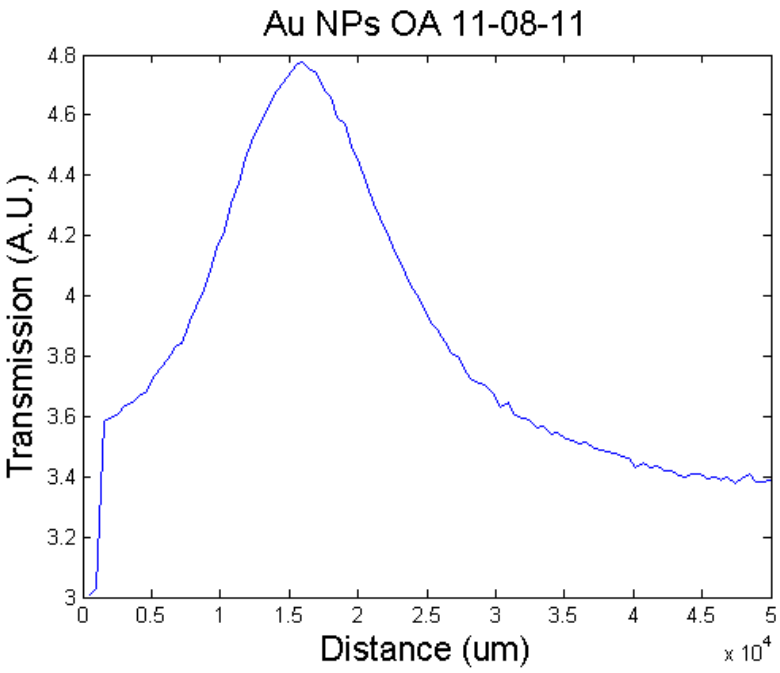

Figure 13 – Open aperture scan of gold nanoparticles imbedded in SiO_2

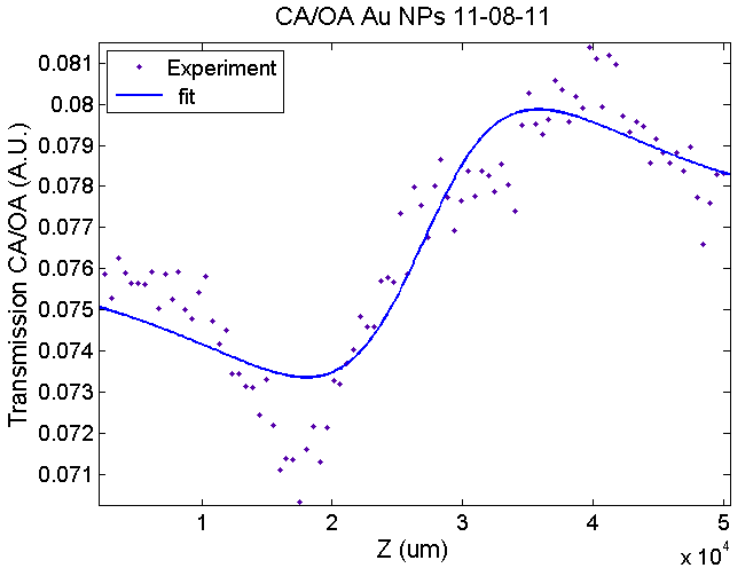

Figure 14 – T_{CA}/T_{OA} for gold nanoparticles imbedded in SiO_2 and fit to equation (18)

Chapter IV

FUTURE WORK

To date, the measurements of n_2 have been performed on VO_x nanoscrolls having the stoichiometry close to V_2O_5. While this is useful, literature suggests that it is possible to reduce such vanadium oxide nanoscrolls to stoichiometric VO_2 and even V_2O_3. Corr, et al., have published results of annealing VO_x nanoscrolls in a 5%:95% H_2:N_2 mixture in a tube furnace at various temperatures and annealing times. The annealing times of 1, 3, and 6 hours were used at temperatures of 400, 500, and 600 ^{0}C. Annealing at 400^{0}C gave monoclinic VO_2 for the annealing times. However, at 500^{0}C, for the three hour annealing time, the authors noticed that the nanoscrolls demonstrated a mixture of monoclinic VO_2 and corundum V_2O_3. Figure 15 shows the resistance versus temperature for three of the annealed samples. Figures 15(a) (1 hour at 400C) and 15(b) (1 hour at 500C) show typical VO_2 hysteresis loops. Figure 15(c) (3 hours at 600C) shows a hysteresis loop for V_2O_3[21].

It is exciting to know that not only has it been shown possible to reduce the VO_x nanoscrolls to stoichiometric VO_2 and V_2O_3, but that there is also evidence of the characteristic phase changes resulting in those stoichiometries of VO_2. Therefore, the future path of research on this project should include obtaining VO_2 nanoscrolls by annealing the VO_x nanoscrolls, followed by measurements of n_2 and α. Furthermore, because the VO_2 nanoscrolls should evidence of the characteristic insulator-metal transition, the attachment of a heating device to the z-scan experiment could allow for the measurement of n_2 and α both above and below the critical temperature of VO_2.

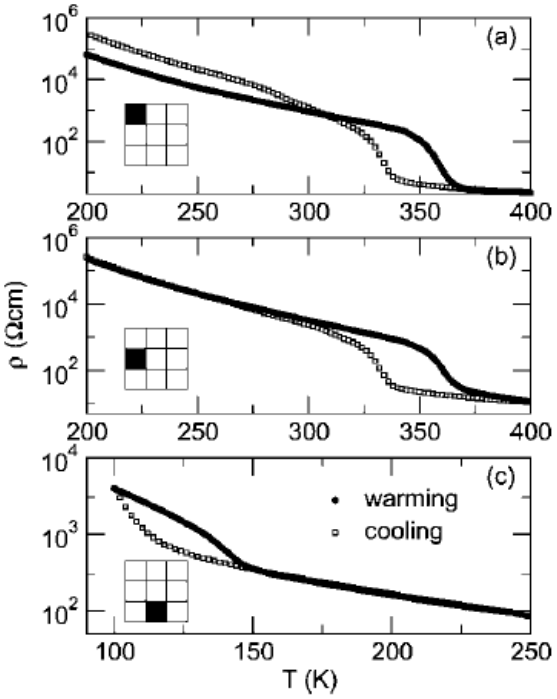

Figure 15 – Hystereses loops measured by Corr, et al, of VO_x nanoscrolls reduced to a) VO_2 at 400C for 1 hour, b) VO_2 at 500C for 1 hour, and c) V_2O_3 at 600C for 3 hours[21].

Furthermore, if the third-order nonlinear index is due to the electrostrictive force on the nanoscrolls and carbon nanotubes, computer simulations would have to involve several components. First, it would have to reproduce the change in density due to the electrostriction of the water and surfactant molecules in the presences of the electric field. Second, it would have to account as well for how strongly the nanotubes and –scrolls are trapped in the laser beam, and how that contributes to the nonlinear index of the material. Third, it would have to explore the interaction strength of the induced dipole in the nanotubes and nanoscrolls with the laser beam. Fourth, it would need to account for any non-linear absorption by both the nanotubes and –scrolls themselves and the liquid in which they are suspended. Fifth, it would have to account for any laser-induced heating in the solution. The good news is that this appears to be a situation where one can divide and conquer, exploring each of these separately before attempting to combine them.

Chapter V

CONCLUSION

Measurements of the nonlinear optical properties are an important step to understanding how to use of Vanadium oxide nanoscrolls as optical limiters. A measurement of the third-order nonlinear refractive index of the nanoscrolls has been made, and is found to be comparable to that comparable to that of multi-wall carbon nanotubes. Because the mechanism behind this third-order nonlinear index is currently unclear, simulations of the system are needed to confirm which of laser-induced heating and electrostriction is the dominant mechanism behind the nanoscroll and nanotube nonlinearities. Meanwhile, implanted gold nanoparticles have a much higher value for n_2, this is because electronic effects of the induced plasmons govern the optical nonlinearity in the nanoparticles. Future progress in the project will involve reduction of the nanoscrolls to stoichiometric VO_2 (and even V_2O_3) to see how the nonlinear optical properties are affected, providing a rich field of research for years to come.

Appendix A

LABVIEW™ PROGRAM

To both collect data from the Picoscope™ and control the motorized stages (translation and rotation), a program was constructed using LabVIEW™ 2009. Figure A-1 shows the front panel of the program. From the front panel, the experiment may be run and parameters of the experiment may be set. From the front panel, one can the number of stops the stage makes along its z-scan sweep, as well as the number of measurements to make at each point. The front panel also gives control over the voltage range of the channels of the Picoscope, as well as the trigger settings of the picoscope. It allows the user to set a path to a folder in which the data files from the experiment are saved. It also allows for interfacing with the translation and rotation stages via Thorlab's GUI, allowing the user to set the position for one while the other is sweeping.

Figures A-2 to A-5 show four quadrants of the block diagram, which is in LabVIEW's graphical programming language.

Figure A-1 -- LABVIEW™ FRONT PANEL

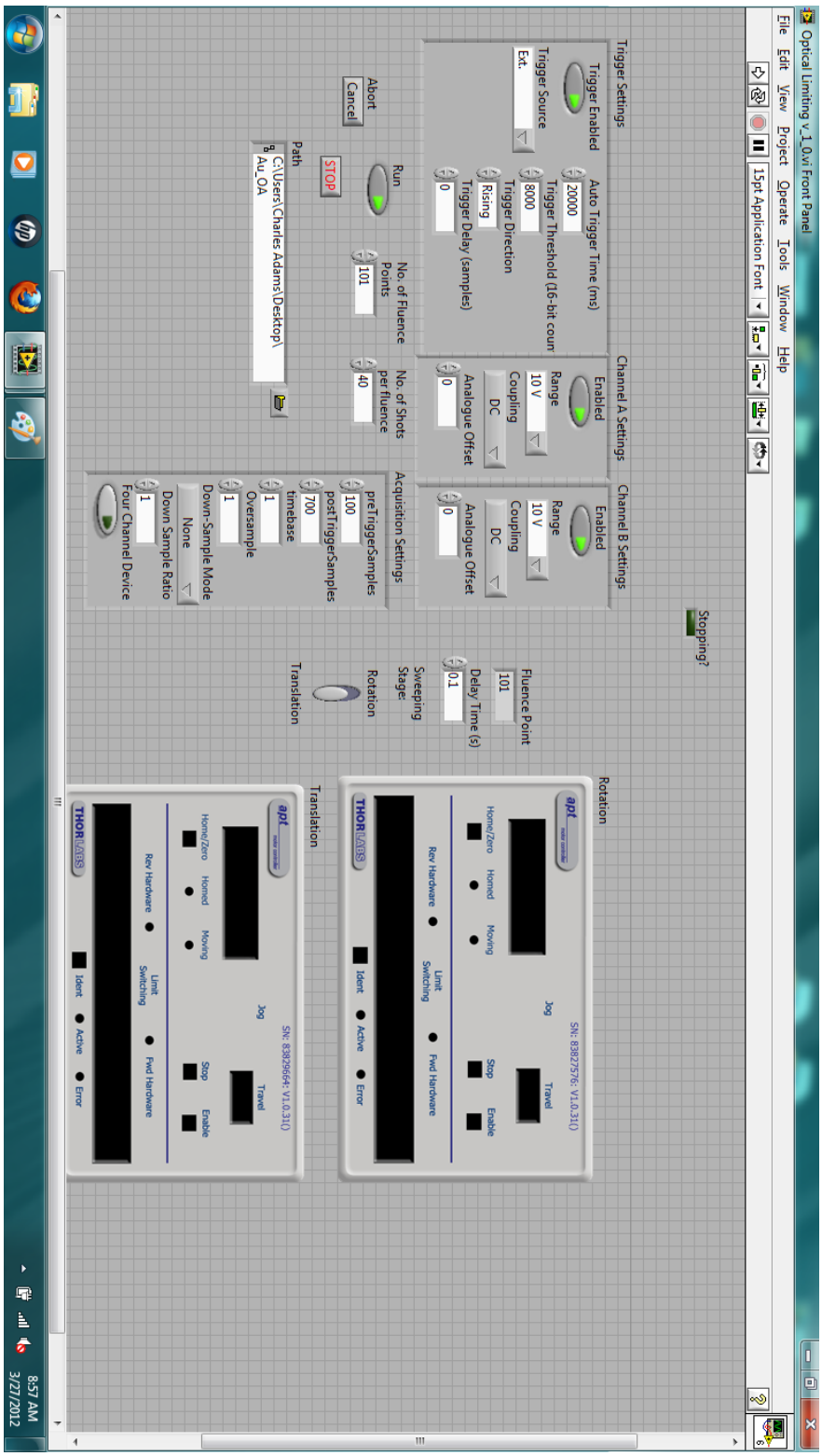

Figure A-2 -- BLOCK DIAGRAM UPPER LEFT

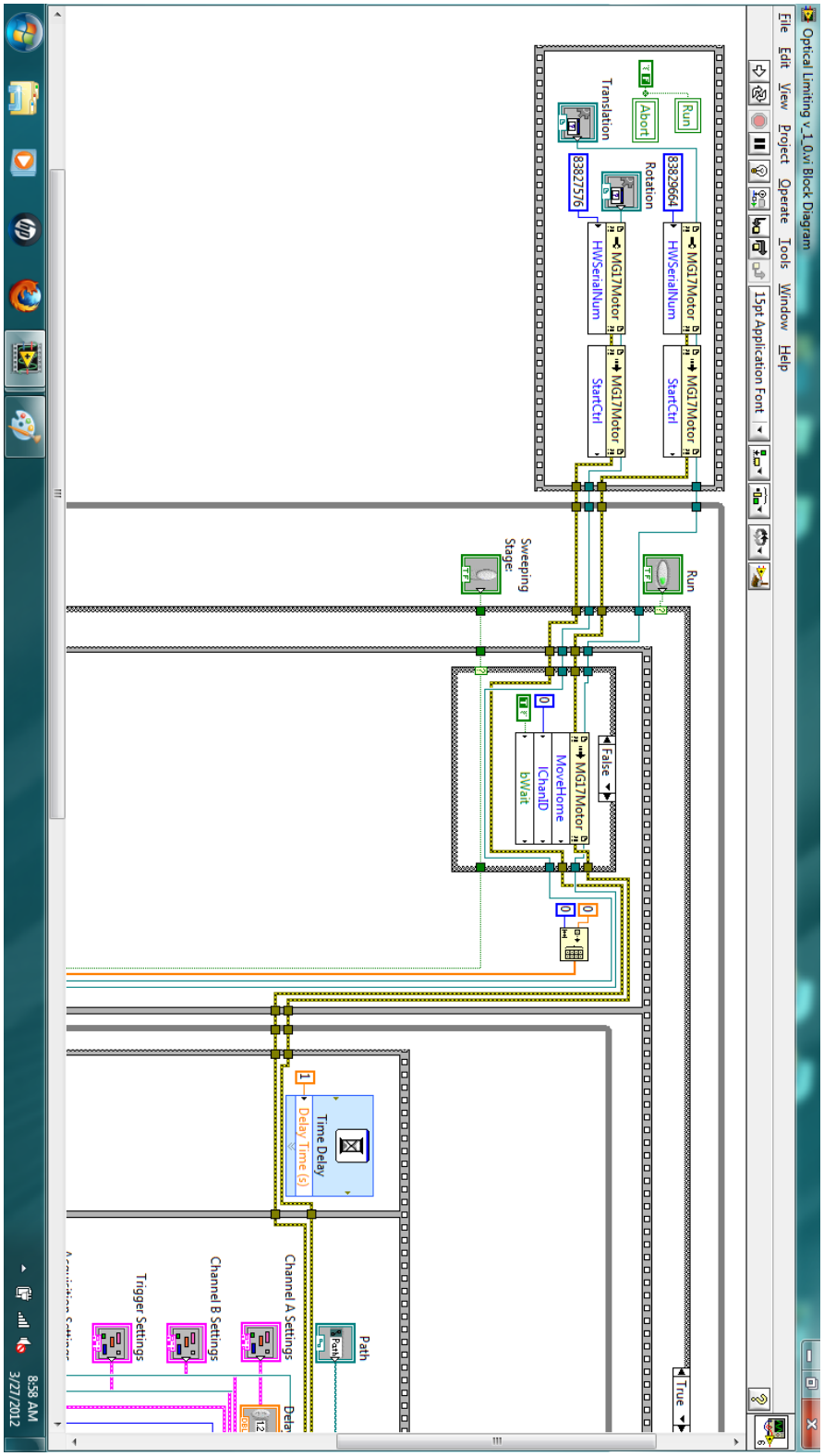

Figure A-3 -- BLOCK DIAGRAM LOWER LEFT

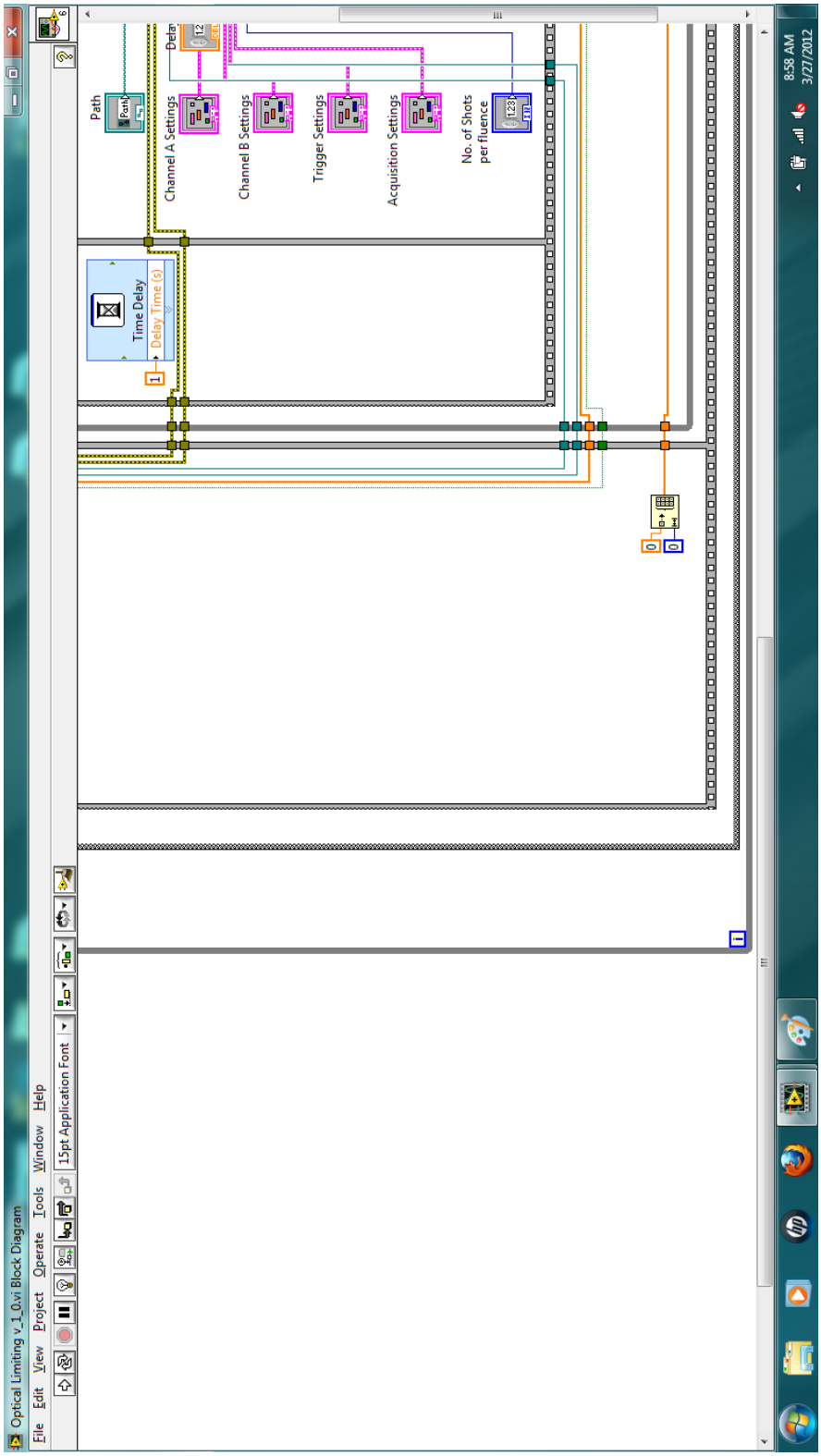

Figure A-4 -- BLOCK DIAGRAM UPPER RIGHT

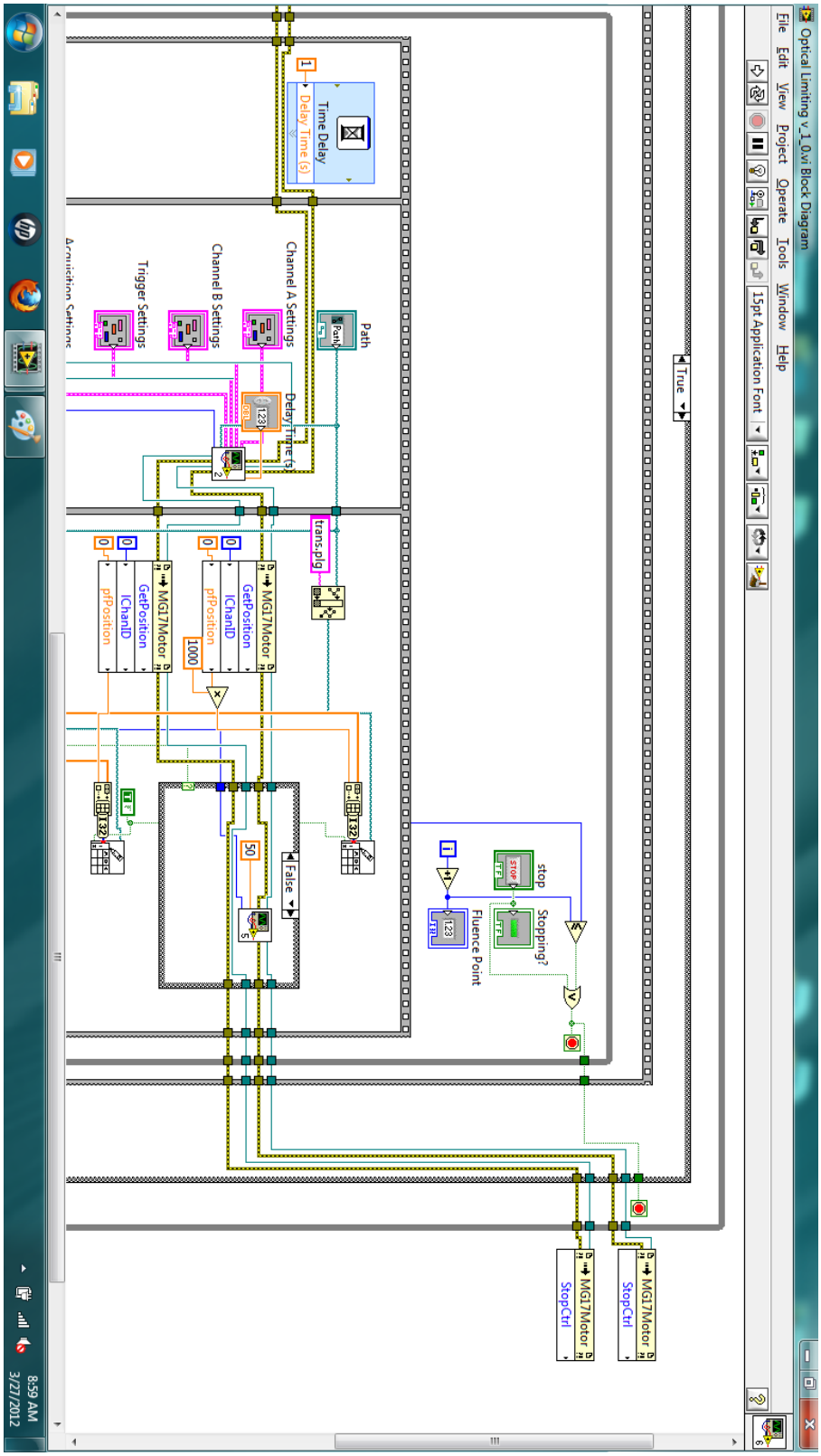

Figure A-5 -- BLOCK DIAGRAM LOWER RIGHT

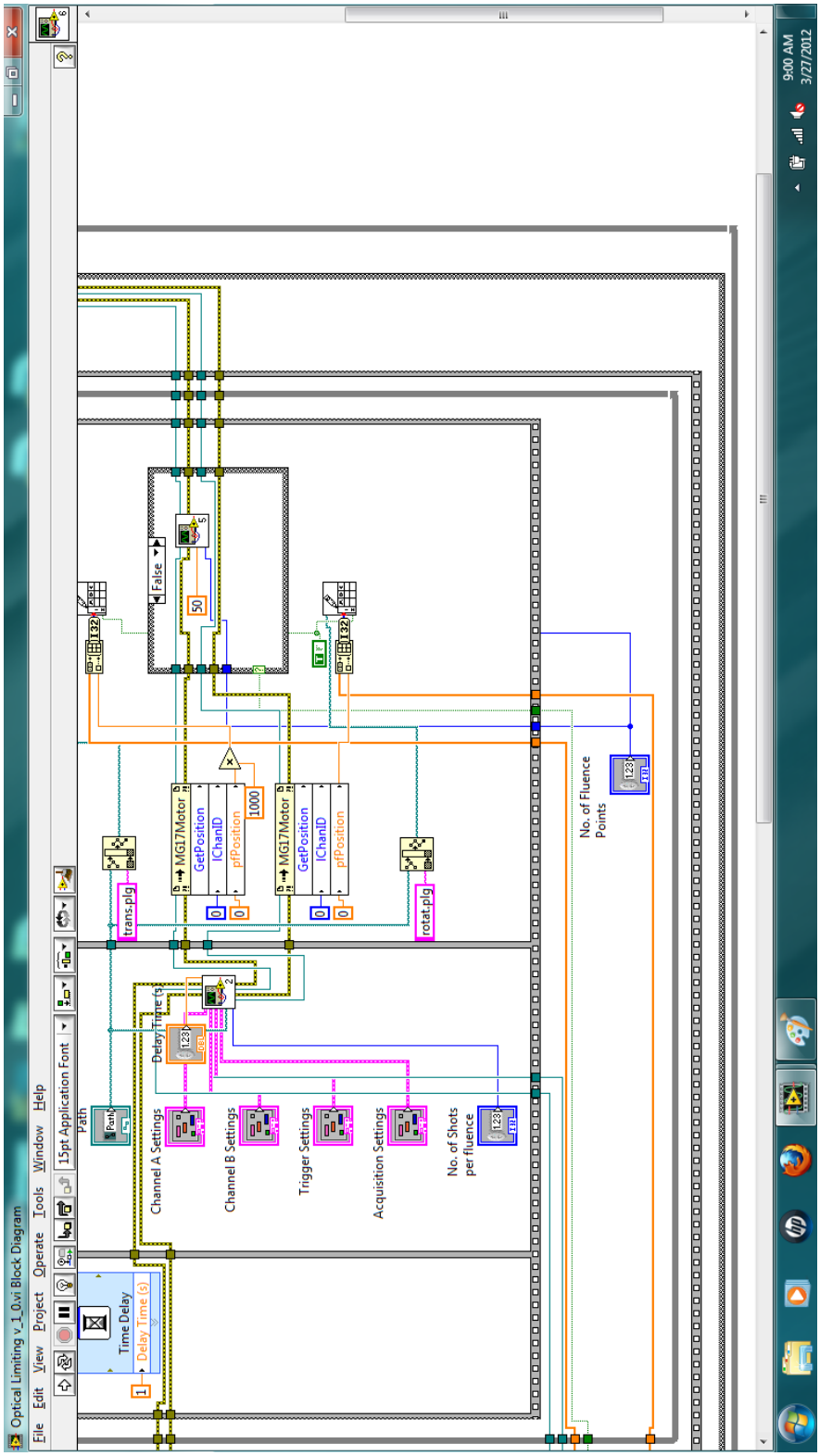

Appendix B

MATLAB™ SCRIPT

This MATLAB™ allows for the speedy analysis of the Picoscope data collected by the LabVIEW program. It will read all the files in a folder of data obtained from a Z-scan run and collate the files by z-position. It then averages the measured intensity for each position for both silicon detector A and silicon detector B (figure 3) and divides the data from A by that from B, to normalize for fluctuations in laser power. It then plots the normalized intensity versus position, as well as outputting that data into a file, for convenient use with MATLAB's fitting tools.

```
%%%%%%%%%%%%%%%%%%%%%%%%%%%%%
%  Optical Limiting Analysis
%
%  input: folder of data with one index file ending in .plg
%
%  output:figures
%
%%%%%%%%%%%%%%%%%%%%%%%%%%%%%

%Variables
polang = 3; % number of digits for polarization
dater = 16; %number of digits before stage position + 1
iter = 40; % number of iterations
saves = 1;
focal = 31.55; %focal spot position
itersize=3;

fil2 = dir('*.plg');
fil = dir('*.txt');

lister = load(fil2(2).name); % use to connect org to actual positon value
lister = lister(:,1);
numofsteps = length(lister);

%% Loading
for n = 1:length(fil)


    temp = fil(n).name;

    itercounter = rem(n-1,iter)+1;
    %itersize = length(num2str(itercounter));
    pos = temp(dater:end-(polang+2+itersize+4));
    position = str2num(pos);
    org = dsearchn(lister,position);
```

```
    datatemp = textread(temp);
    channel1(org,itercounter,:) = datatemp(:,1); % (index corresponding to
postion, iteration number, data)
    channel2(org,itercounter,:) = datatemp(:,2);
end

%% Formatting


avgchannel1 = mean(channel1,2);
avgchannel2 = mean(channel2,2);
maxchannel1 = max(avgchannel1,[],3);
maxchannel2 = max(avgchannel2,[],3);

for k=1:length(lister)
    Y(k,1)=maxchannel1(k,1)/maxchannel2(k,1);
end
saver(:,1)=lister(:,1);
saver(:,2)=Y(:,1);
%% Plotting

figure;
scatter(lister(1:length(lister)), Y(1:length(lister)), 16,'filled');
xlabel('Z (\mum)','fontsize',16);
ylabel('Transmission (A.U.)','fontsize',16);
title('VO_x NTs OA','fontsize',16);

    if saves == 1
    dlmwrite('VOxOA_1208.dat',saver,'\t')
    end
```

Appendix C

KNIFE-EDGE MEASUREMENTS

This appendix contains measurements of beam width made using the knife-edge methodology. Note the persistent edge throughout all the knife-edge measurements indicating a deviation from a Gaussian beam.

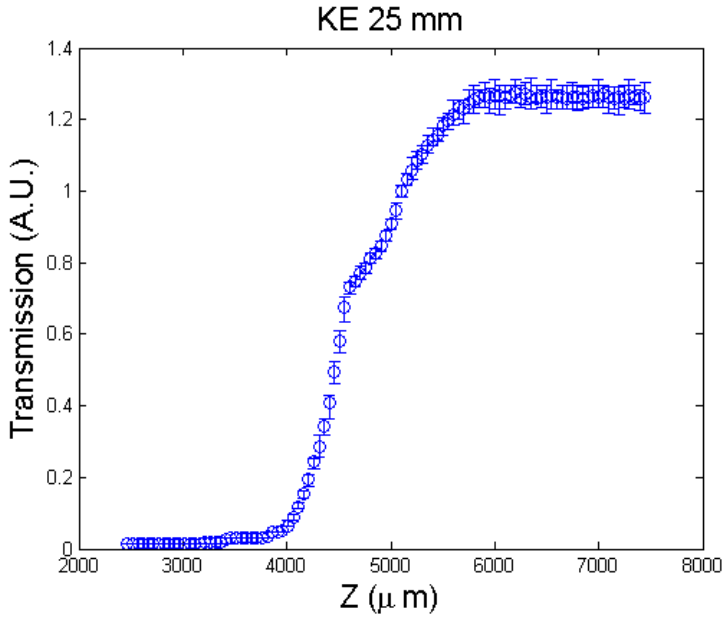

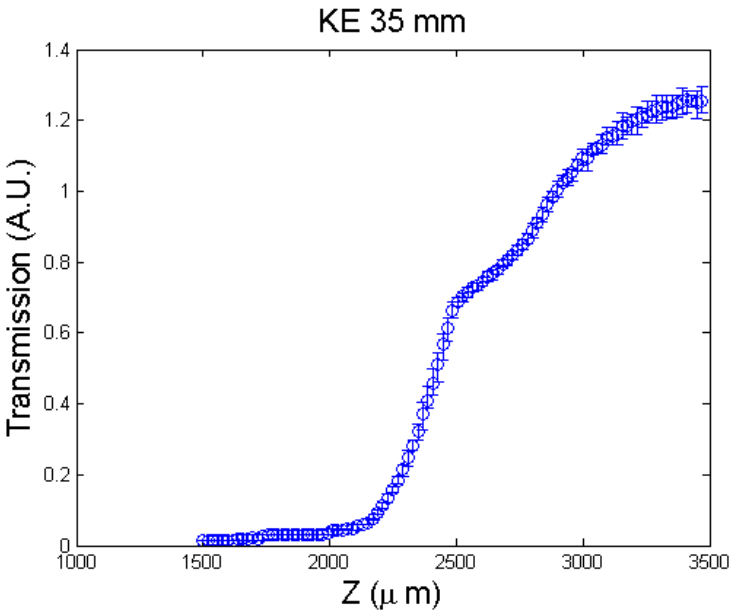

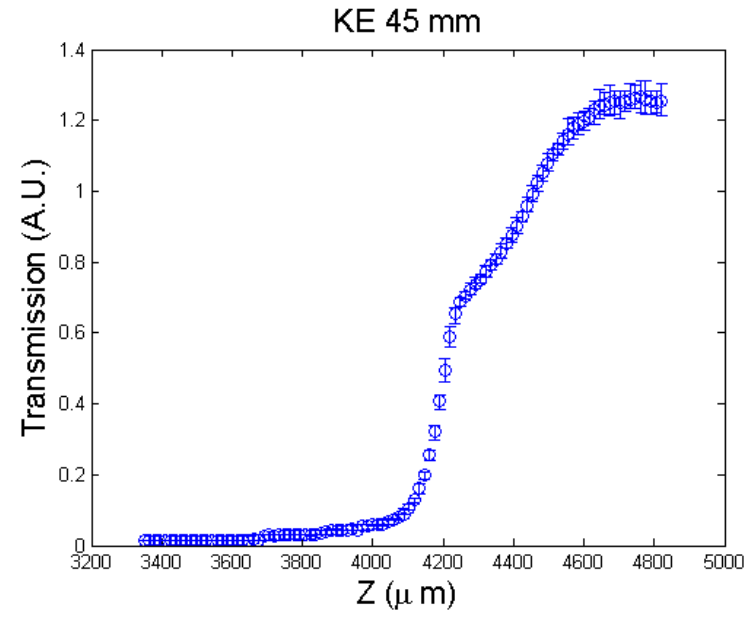
KE 45 mm
Transmission (A.U.)
Z (μ m)
0
0.2
0.4
0.6
0.8
1
1.2
1.4
3200
3400
3600
3800
4000
4200
4400
4600
4800
5000

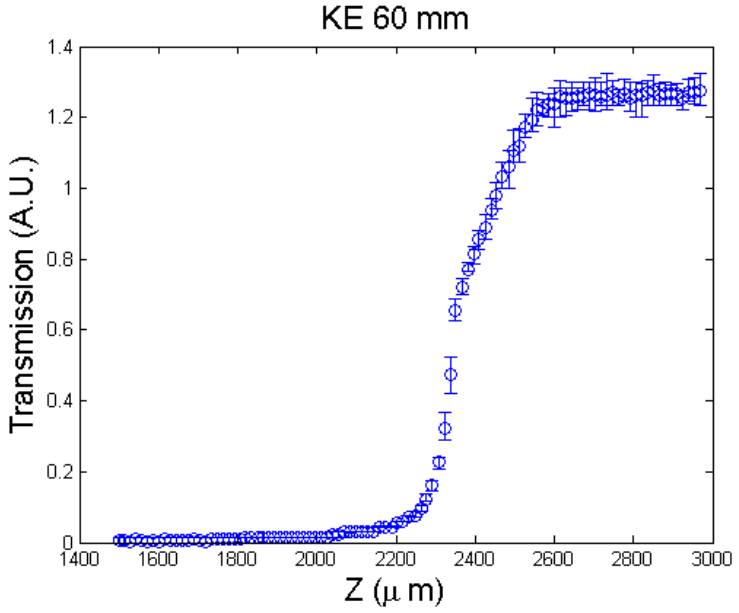
KE 60 mm
Transmission (A.U.)
Z (μ m)
0
0.2
0.4
0.6
0.8
1
1.2
1.4
1400
1600
1800
2000
2200
2400
2600
2800
3000

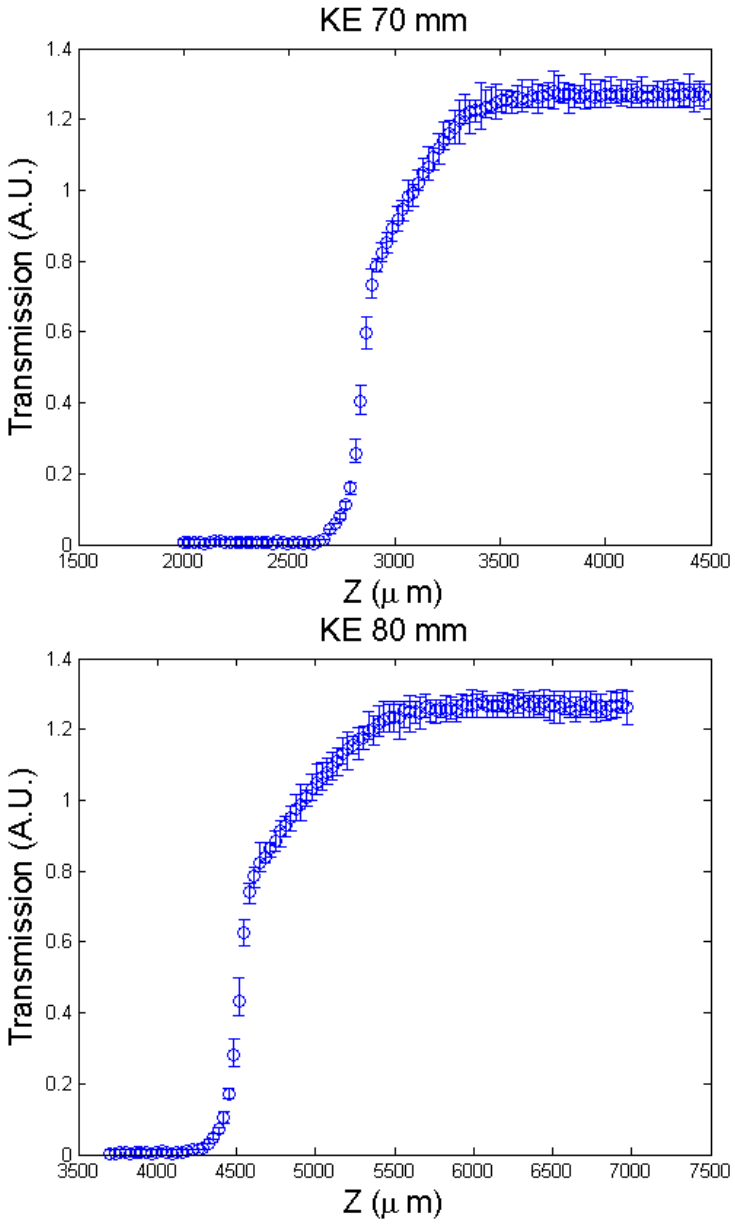

Figure C-1. Knife-edge measurement for various distances from the focal lens.

REFERENCES

1. M. Maaza, D. Hamidi, A. Simo, T. Kerdja, A. K. Chaudhary and J. B. K. Kana, "Optical limiting in pulsed laser deposited VO2 nanostructures," *Optics Communications*, 285 (6), 1190-1193
2. Y. Gao, S. Wang, H. Luo, L. Dai, C. Cao, Y. Liu, Z. Chen and M. Kanehira, "Enhanced chemical stability of VO2 nanoparticles by the formation of SiO2/VO2 core/shell structures and the application to transparent and flexible VO2-based composite foils with excellent thermochromic properties for solar heat control," *Energy & Environmental Science*, 5 (3), 6104-6110
3. M. R. Parida, C. Vijayan, C. S. Rout, C. S. S. Sandeep, R. Phiip and P. C. Deshmukh, "Room Temperature Ferromagnetism and Optical Limiting in V(2)O(5) Nanoflowers Synthesized by a Novel Method," *Journal of Physical Chemistry C*, 115 (1), 112-117
4. H. Coy, R. Cabrera, N. Sepulveda and F. E. Fernandez, "Optoelectronic and all-optical multiple memory states in vanadium dioxide," *Journal of Applied Physics*, 108 (11),
5. R. W. Boyd, *Nonlinear Optics*, Elsevier, Inc., Amsterdam, 2008.
6. A. Cheremisin, V. Putrolaynen, A. Velichko, A. Pergament, N. Kuldin and A. Grishin, "UV laser modification and selective ion-beam etching of amorphous vanadium pentoxide thin films," *Physica Status Solidi a-Applications and Materials Science*, 206 (7), 1484-1487 (2009).
7. V. V. Putrolaynen, A. A. Velichko, A. L. Pergament, A. B. Cheremisin and A. M. Grishin, "UV patterning of vanadium pentoxide films for device applications," *Journal of Physics D-Applied Physics*, 40 (17), 5283-5286 (2007).
8. J. Nag and R. F. Haglund, "Synthesis of vanadium dioxide thin films and nanoparticles," *Journal of Physics-Condensed Matter*, 20 (26), (2008).
9. J. Nag, "The Solid-Solid Phase Transition in Vanadium Dioxide Thin Films: Synthesis, Physics and Application," *Physics*, Vanderbilt University: Nashville, TN, 192 (2011)

10. J. F. Xu, R. Czerw, S. Webster, D. L. Carroll, J. Ballato and R. Nesper, "Nonlinear optical transmission in VOx nanotubes and VOx nanotube composites," *Applied Physics Letters*, 81 (9), 1711-1713 (2002).
11. E. U. Donev, R. Lopez, L. C. Feldman and R. F. Haglund, "Confocal Raman Microscopy across the Metal-Insulator Transition of Single Vanadium Dioxide Nanoparticles," *Nano Letters*, 9 (2), 702-706 (2009).
12. K. Appavoo, D. Y. Lei, Y. Sonnefraud, B. Wang, S. T. Pantelides, S. A. Maier and R. F. Haglund, "Role of Defects in the Phase Transition of VO2 Nanoparticles Probed by Plasmon Resonance Spectroscopy," *Nano Letters*, 12 (2), 780-786
13. J. Wei, Z. Wang, W. Chen and D. H. Cobden, "New aspects of the metal-insulator transition in single-domain vanadium dioxide nanobeams," *Nature Nanotechnology*, 4 (7), 420-424 (2009).
14. F. Krumeich, H. J. Muhr, M. Niederberger, F. Bieri, B. Schnyder and R. Nesper, "Morphology and topochemical reactions of novel vanadium oxide nanotubes," *Journal of the American Chemical Society*, 121 (36), 8324-8331 (1999).
15. H. J. Zhang, J. H. Dai, P. Y. Wang and L. A. Wu, "Self-Focusing and Self-Trapping in New Types of Kerr Media with Large Nonlinearities," *Optics Letters*, 14 (13), 695-696 (1989).
16. A. Ashkin, "Applications of Laser-Radiation Pressure," *Science*, 210 (4474), 1081-1088 (1980).
17. C. Bustamante, Z. Bryant and S. B. Smith, "Ten years of tension: single-molecule DNA mechanics," *Nature*, 421 (6921), 423-427 (2003).
18. M. Sheikbahae, A. A. Said, T. H. Wei, D. J. Hagan and E. W. Vanstryland, "Sensitive Measurement of Optical Nonlinearities Using a Single Beam," *Ieee Journal of Quantum Electronics*, 26 (4), 760-769 (1990).
19. M. Sheikbahae, A. A. Said, D. J. Hagan, M. J. Soileau and E. W. Vanstryland, "Nonlinear Refraction and Optical Limiting in Thick Media," *Optical Engineering*, 30 (8), 1228-1235 (1991).

20. A. S. Laryushkin, V. V. Savel'ev, V. I. Zolotarevskii, A. D. Grishina, T. V. Krivenko, R. W. Rychwalski and A. V. Vannikov, "Third-order optical susceptibility of single-walled carbon nanotubes," *High Energy Chemistry*, 45 (3), 245-249

21. S. A. Corr, M. Grossman, J. D. Furman, B. C. Melot, A. K. Cheetham, K. R. Heier and R. Seshadri, "Controlled Reduction of Vanadium Oxide Nanoscrolls: Crystal Structure, Morphology, and Electrical Properties," *Chemistry of Materials*, 20 (20), 6396-6404 (2008).

22. SES Research. https://sesres.com/Nanotubes.asp. 12 November 2012.

23. *Minilite™ Operation Manual*, Continuum Electro-Optics, Inc., Santa Clara, CA, 1997.

24. "MATLAB™ Help File Search "Nonlinear Least Squares.""

25. N. Pincon, B. Palpant, D. Prot, E. Charron and S. Debrus, "Third-order nonlinear optical response of Au : SiO2 thin films: Influence of gold nanoparticle concentration and morphologic parameters," *European Physical Journal D*, 19 (3), 395-402 (2002).

26. A. I. Ryasnyanskiy, B. Palpant, S. Debrus, U. Pal and A. L. Stepanov, "Nonlinear Optical Properties of Gold Nanoparticles Dispersed in Different Optically Transparent Matrices," *Physics of the Solid State*, 51 (1), 55-60 (2009).